Master Thesis

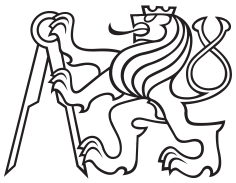

Czech Technical University in Prague

F3

Faculty of Electrical Engineering
Department of Control Engineering

H_2 optimal control algorithms for vehicle control

David Vošahlík

Supervisor: Ing. Tomáš Haniš, Ph.D.
Field of study: Cybernetics and Robotics
Subfield: Cybernetics and Robotics
January 2020

ZADÁNÍ DIPLOMOVÉ PRÁCE

I. OSOBNÍ A STUDIJNÍ ÚDAJE

Příjmení: **Vošahlík** Jméno: **David** Osobní číslo: **439578**

Fakulta/ústav: **Fakulta elektrotechnická**

Zadávající katedra/ústav: **Katedra řídicí techniky**

Studijní program: **Kybernetika a robotika**

Studijní obor: **Kybernetika a robotika**

II. ÚDAJE K DIPLOMOVÉ PRÁCI

Název diplomové práce:

H2 optimal control algorithms for vehicle control

Název diplomové práce anglicky:

H2 optimal control algorithms for vehicle control

Pokyny pro vypracování:

The goal of the thesis is to investigate control algorithms for land vehicles in order to develop full-time and full-authority control system. H2 optimization based methodology will be employed in order to investigate inovative control strategies and vehicle maneuver parametrization and execution. The thesis will be done in following steps:
1. Adopt non-linear verification mathematical model (Matlab&Simulink, Vehicle Dynamics Block-set).
2. Derivation of design model suitable for H2 algorithms.
3. Principal investigation of vehicle maneuver parametrization.
4. Control system problem formulation suitable for H2 methodology.
5. Implementation of control algorithms in Matlab & Simulink.
6. Control algorithms verification based on virtual riding tests.

Seznam doporučené literatury:

[1] Dieter Schramm, Manfred Hiller, Roberto Bardini – Vehicle Dynamics – Duisburg 2014
[2] Hans B. Pacejka - Tire and Vehicle Dynamics – The Netherlands 2012
[3] K. Zhou, J.C. Doyle, and K. Glover, Robust and Optimal Control. Englewood Cliffs, NJ: Prentice Hall, 1996
[4] Skogestad, Sigurd & Postlethwaite, I. (2005). Multivariable Feedback Control: Analysis and Design

Jméno a pracoviště vedoucí(ho) diplomové práce:

Ing. Tomáš Haniš, Ph.D., katedra řídicí techniky FEL

Jméno a pracoviště druhé(ho) vedoucí(ho) nebo konzultanta(ky) diplomové práce:

Datum zadání diplomové práce: **11.07.2019** Termín odevzdání diplomové práce: _____

Platnost zadání diplomové práce: **19.02.2021**

Ing. Tomáš Haniš, Ph.D.	prof. Ing. Michael Šebek, DrSc.	prof. Mgr. Petr Páta, Ph.D.
podpis vedoucí(ho) práce	podpis vedoucí(ho) ústavu/katedry	podpis děkana(ky)

III. PŘEVZETÍ ZADÁNÍ

Diplomant bere na vědomí, že je povinen vypracovat diplomovou práci samostatně, bez cizí pomoci, s výjimkou poskytnutých konzultací. Seznam použité literatury, jiných pramenů a jmen konzultantů je třeba uvést v diplomové práci.

. _____ Podpis studenta

Datum převzetí zadání

Acknowledgements

I would like to thank Ing. Tomáš Haniš, Ph.D. for his counsel and for his selfless and devoted attitude towards his students.

I would also like to thank to Ing. Denis Efremov with his help in introduction to his single track vehicle model.

Mainly I would like to thank my whole family for their everlasting love and support. Without them, this work couldn't ever originate.

Declaration

I declare that the presented work was developed independently and that I have listed all sources of information used within it in accordance with the methodical instructions for observing the ethical principles in the preparation of university theses.

Prague, date 7. January 2020

.....
signature

Abstract

Trend of autonomous vehicles and e-mobility is in favor of an advanced control system development and deployment. Vehicle dynamics level control systems providing safety limits and high performance response, especially during high dynamics maneuvers, are necessary. This work provides solution for vehicle longitudinal dynamics (vehicle acceleration) considering physical limits given by road, tire and vehicle dynamics respectively. The goal is to maximize vehicle longitudinal acceleration. Considered mathematical model is nonlinear single-track model incorporating nonlinear Pacejka magic formula as a tire model. This work proposes two possible control approaches.

In first part the direct longitudinal slip ratio λ control is presented. Design model for control system is derived as a linearized state-space model at constant acceleration operation point. Therefore, the common linearization approach, at system equilibrium, is not possible and the linearization along system trajectory is used. Such solution results in involvement of LPV techniques, as vehicle velocity is state variable. Next, the LQ optimal control framework is employed to deliver control algorithms providing constant longitudinal slip ratio trajectory tracing.

Augmented direct slip ratio λ control based on wheel angular velocity tracking is proposed in second part. The core of suggested hierarchical control system is the LQ-based closed loop for single wheel angular velocity ω tracking. The ω setpoint signal is computed based on λ demand. Finally, the vehicle longitudinal acceleration controller is designed. Virtual riding tests comparing the ω tracking based control system and open loop behavior on slippery surface are provided at the end of thesis.

Keywords: Single-track model, vehicle, acceleration control, slip ratio control, LQ based control, gain scheduling control

Supervisor: Ing. Tomáš Haniš, Ph.D.

Abstrakt

Vzestup autonomních vozidel a e-mobility umožňuje nasazení pokročilých řídicích systémů. Řízení na úrovni dynamiky vozidla poskytuje vyšší bezpečnost a lepší odezvu speciálně při velmi rychlých manévrech. Tato práce bere v potaz fyzikální limity dané cestou, pneumatikami a dynamikou vozidla a navrhuje řešení pro řízení podélné dynamiky. Cílem je maximalizovat podélné zrychlení vozidla. V této práci je použit jako nelineární verifikační a validační model jednostopý model vozidla, který zahrnuje Pacejkovu magickou rovnici pro modelování pneumatik. Jsou zde navrženy 2 možné přístupy k řešení.

V první části je prezentováno řízení podélného skluzu λ. Stavový model pro návrh řídicího systému je odvozen z nelineárního modelu v pracovním bodě s konstantním zrychlením. Protože rychlost je stav systému nelze zde použít běžné linearizační metody - nejedná se o linearizaci v ekvilibriu. Místo toho je použita linearizace podél trajektorie. Toto výustí v použití LPV technik. Dále je navržen řídicí algoritmus založený na použití LQ metodologie, který řídí podélný skluz.

V druhé části je představen řídicí systém založený na sledování úhlové rychlosti kol. Jádro tohoto systému tvoří zpětnovazební LQ řídicí smyčka pro řízení úhlové rychlosti ω kola. Referenční signál ω_{Ref} je vypočítáván na základě požadavku na λ. Jako nejvyšší v hierarchii je zpětnovazební smyčka řízení zrychlení. Nakonec jsou provedeny virtuální jízdní testy, které porovnávají řídicí sytém založený na sledování ω_{Ref} a systém bez regulace na klouzavém povrchu.

Klíčová slova: jednostopý model vozidla, vozidlo, řízení zrychlení, řízení podélného skluzu, řízení založené na LQ, řízení založené na přepínání zesílení

Překlad názvu: Řídicí systém dynamiky vozu založený na H_2 algoritmech

Contents

Figures

Tables

Chapter 1

Introduction

Word vehicle comes from the Latin word vehiculum which means "a machine that transports people or cargo". That word includes all possible types of vehicles like e.g. planes, boats, cars, motorbikes and many others. This thesis is concerning only to the land vehicles namely to personal cars.

The history of cars is quite long. The first car was built in about 1769 by french inventor Nicolas-Joseph Cugnot. It was the first full-scale, self-propelled mechanical car. It was powered with steam. As the time was running also another types of cars were developed and built. Nowadays cars have many different types of power and are of many different shapes and faces. In the interest of this work are exclusively the cars with four wheels and electrical or hybrid powertrain. This is due to fact that these types of powertrain offer wider bandwidth in torque delivery than the widely used combustion engine.

Furthermore this work is about controlling the longitudinal dynamics of such cars. This work admits some non-conform mechanical configurations of a car which couldn't be possible to control directly by man. This is because the system (non-conform car) is quite beyond the man ability to control it (high frequencies, many inputs and outputs,...). More about this can be found further in the work. In next subsection the goals of this work are laid down.

Part of this thesis was also presented on 22nd International Conference on Process Control (PC19). The paper which was presented there is [VHH19]. More details can be found in the upcoming sections. Mainly it was the part that is covered by Chapter 4. Another part of thesis was submitted for 21st

IFAC World Congress in Berlin. This part is mostly described in Chapter 5.

1.1 Goals

The premises for the presented goals are described above. These are in abbreviation electrical or hybrid power-train (brings the opportunity for advanced control with torque delivery wider bandwidth compared to classical combustion engine), four-wheeled land vehicle with every wheel capable of independent steering angle and having independent torque delivery (engine). In this work the single-track model is considered so only 2 wheels each capable of independent steering angle and 2 engines (electrical) are used.

The assignment points of this thesis are following:

1. Adopt and implement nonlinear control design and validation vehicle model.
2. Derive design model suitable for the H2 algorithms.
3. Investigate principal vehicle-maneuver parametrization
4. Formulate the control problem that will be suitable for the H2 methodology.
5. Implement the developed control algorithms in Matlab/Simulink using Vehicle Dynamics Block-set
6. Verificate the algorithms based on the virtual riding tests.

Table 1.1: Assignment of the thesis.

From the table Table 1.1 is clear that this thesis should use H_2 optimal control. This goal is fulfilled using the deterministic LQ (linear quadratic) control. The fact that the deterministic LQ control is special case of H_2 optimal control is proven in many publications. E.g. in [GC03] can be found rigorous proof of this fact. Also in [SS05, Chapter 8] can be found discussion regarding this fact.

For sake of simplicity of the designed controllers the LQ control is used for infinite time horizon. That means the controllers shrinks to simple state feedback (details can be found e.g. in [SS05]).

The main advantage of using infinite time horizon LQ is its simplicity of static state feedback compared to dynamic controllers that are results of general H_2 methodology.

1.2 Structure

This work has following structure:

Chapter 2	Principal maneuver parametrization.
Chapter 3	Nonlinear vehicle model used for derivation of control design model and controller verification.
Chapter 4	Derivation of design model and successive controller design using gain scheduling and LQ techniques for longitudinal slip ratio tracking.
Chapter 5	Alternative acceleration/slip ratio tracking, based on wheel angular velocity tracking.
Chapter 6	Validation and verification of the designed controllers using nonlinear model. Virtual riding tests results are presented here.

Chapter 2

Maneuver Principal Parametrization

In this chapter the overall goals and possibilities of the controlled signals will be layed down. The goal of this section is to propose the reference signals most convenient for the human, to drive a vehicle with in this thesis delivered control system.

Nowadays the main inputs, which are man handled, to the vehicle system that control the dynamic behavior are clear:

- accelerator pedal
- brake pedal
- steering wheel

Steering is not in scope of this thesis as only the longitudinal dynamics is considered with its range for the thesis.

First let's talk about the accelerator and brake pedal, these two corresponds to each other in the way that both are used for acceleration. This thesis deals mainly with positive acceleration in the meaning that the vehicle is increasing the velocity. But in principle the reference signal coming from the brake pedal would be handled in the same way as reference from accelerator pedal.

2.1 Accelerator and brake pedal

Currently with usage of combustion engine (the most common situation) the accelerator pedal is for controlling the fuel flow to the engine. This corresponds to the torque applied on the driven wheels. The torque characteristics comparison for combustion and electrical drivetrain can be seen on the figure Fig. 2.1. The power limitations that can be seen for higher velocities are unavoidable. Nevertheless the pedal signal corresponds to demanded torque. This is also applicable for most of the electrical and hybrid drivetrains.

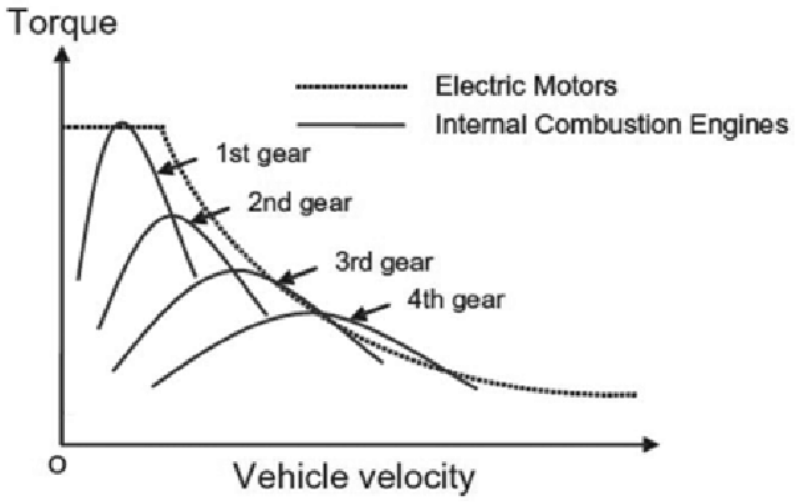

Figure 2.1: Comparison of torque characteristics for combustion and electrical engine. The figure was adopted from [ZLH+17]

The first thought that comes to mind is to create system that will track the torque reference. What if we go further and make a system that will track the acceleration as it has many advantages. The driver is not capable and also willing to be aware of the riding surface condition e.g. is there ice on the road or not, or is there a puddle that the vehicle is going through? The acceleration force is according to the Pacejka's magic formula (introduced in Section 3.2.2) dependent on the wheel longitudinal slip ratio λ.

Let us consider the reference signal coming from the accelerator pedal the slip ratio reference λ_{Ref}. This already decouples the reference signal from the riding surface properties as was described above and is straightforward (from controller point of view) to control compared to vehicle acceleration. Longitudinal slip ratio also corresponds to the ratio of available traction force/acceleration. A limit was set on λ_{Ref} (described in Chapter 4 and Chapter 5) that equals to maximum available acceleration that can be different for snow, asphalt and others, while λ remains more or less constant.

This approach is used in both Chapter 4 and Chapter 5. In Chapter 5 the control system proposed is further improved with acceleration control. However only a simple proof of concept is introduced there.

Not depending on what is controlled (acceleration or slip ratio) it can be used for controlling both - acceleration and braking/deceleration. The reference signals coming from the pedals can be subtracted from each other and the resulting signal will be fed to the acceleration/longitudinal slip ratio control system. Both pedals are covered in this way. This concept is shown in the figure Fig. 2.2

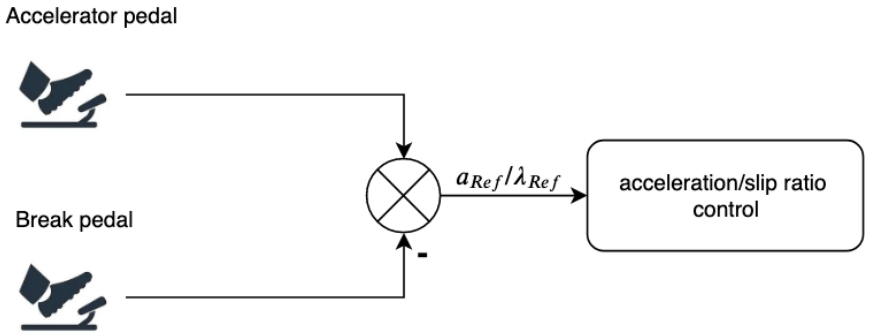

Figure 2.2: Proposed accelerator and brake pedal control architecture.

Chapter 3

Nonlinear Vehicle Model

3.1 Introduction

The Nonlinear high-fidelity model is needed for derivation of design model used for control laws development. It is also used for verification of proposed control laws. There are mainly two models that are widely accepted in the automotive community - single-track model and twin-track model. Twin-track model derivation can be found in [SHB14, Chapter 10] and [Cib19]. This model is more complex compared to the single-track one (it has 4 wheels against only two wheels in single-track), but for purposes of this thesis single-track model is sufficient (as mostly the longitudinal dynamics of a vehicle is studied). The single-track model was also used in many papers as high-fidelity model e.g. [Ack94, GGK08, WA98].

The single-track model is in this thesis considered as high-fidelity nonlinear model. The single-track model is derived in [Efr18] and in [SHB14, Chapter 9]. The model was also used in [VHH19]. For the convenience of the reader the model is here introduced. The introduced model is for purposes of the thesis augmented by physical phenomena that weren't modeled in [VHH19] (described in following sections). This single-track model was implemented in Matlab/Simulink and was used for further control design.

3.2 Single-track model

The single-track model is used to describe planar motion of a vehicle (car) using only two wheels. One wheel common for both front wheels and one for both rear wheels. Rotational rear wheel is considered in this adopted model. There are some simplifications and assumptions which were used during model derivation. These are:

- Lifting, rolling and pitching motion is neglected.
- Both front wheels are represented as single wheel, this is also applicated for both rear wheels.
- Powertrain dynamics is neglected. Inputs to the system are directly the torques acting on the wheels.

Vehicle coordinate system used is conventional right hand oriented cartesian coordinate system with x axis in direction of travel and z axis pointing upwards. The system can be seen in figure Fig. 3.1.

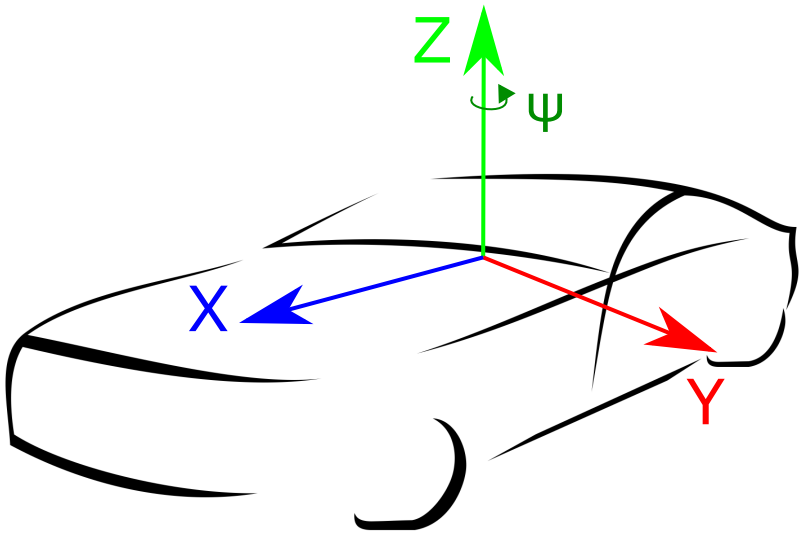

Figure 3.1: Vehicle coordinate system used. The picture was adopted from [Efr18]

The single-track model scheme with all simplifications and assumptions mentioned above is presented in the figure Fig. 3.2.

The model state space description is based on following equations of motion:

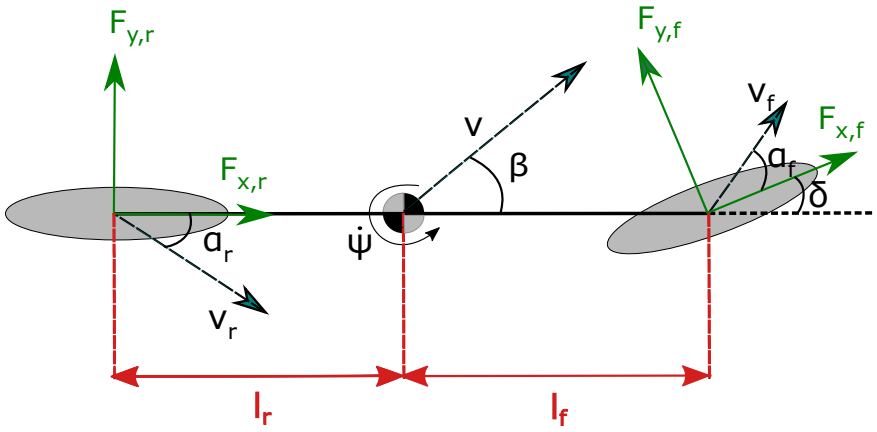

Figure 3.2: Single-track nonlinear model. The picture was adopted from [Efr18]

- Longitudinal motion

$$-mv\left(\dot{\beta}+\dot{\psi}\right)sin\left(\beta\right)+m\dot{v}cos\left(\beta\right)=F_x \tag{3.1}$$

- Lateral motion

$$mv\left(\dot{\beta}+\dot{\psi}\right)cos\left(\beta\right)+m\dot{v}sin\left(\beta\right)=F_y \tag{3.2}$$

- Yaw motion

$$I_z\ddot{\psi}=M_z \quad . \tag{3.3}$$

Where β is sideslip angle, m is vehicle's mass, v is velocity of the vehicle's center of gravity (CG), $\dot{\psi}$ is yaw rate of the vehicle, F_x is longitudinal force (acting in x direction) acting on the CG, F_y is lateral force (acting in y direction) acting on the CG, I_z is moment of inertia of the vehicle around its z axis in CG and M_z is cornering torque acting in the CG around the z axis.

These equations of motion can be rewritten into the state space description in following manner

$$\dot{\beta}=-\dot{\psi}+\frac{1}{mv}\left(cos\left(\beta\right)F_y-sin\left(\beta\right)F_x\right) \tag{3.4}$$

$$\dot{v}=\frac{1}{m}\left(sin\left(\beta\right)F_y+cos\left(\beta\right)F_x\right) \tag{3.5}$$

$$\ddot{\psi}=\frac{1}{I_z}M_z \quad . \tag{3.6}$$

The forces acting on the vehicle are

$$F_x=cos\delta_f F_{xf}-sin\delta_f F_{yf}+cos\delta_r F_{xr}-sin\delta_r F_{yr} \tag{3.7}$$

$$F_y=sin\delta_f F_{xf}+cos\delta_f F_{yf}+sin\delta_r F_{xr}+cos\delta_r F_{yr} \tag{3.8}$$

$$M_z=l_f\ sin\delta_f F_{xf}+l_f\ cos\delta_f F_{yf}+l_r\ sin\delta_r F_{xr}-l_r\ cos\delta_r F_{yr} \quad . \tag{3.9}$$

Here F_{xf} and F_{yf} are forces acting on the front wheel in x and y direction. F_{xr} and F_{yr} are forces acting on the rear wheel. δ_f and δ_r are inputs to the system, these are steering angles of the front and rear wheel respectively.

3.2.1 Wheel model

Wheel coordinate system is used for the wheel dynamics description. This coordinate system is depicted in figure Fig. 3.3.

The wheels' dynamics is described with the equations

$$\dot{\omega}_f = \frac{1}{J_f}\left(\tau_f - R_f F_{xf} - sign\left(\omega_f\right)\tau_{Bf} - k_f v_{xf}\right) \quad , \tag{3.10}$$

$$\dot{\omega}_r = \frac{1}{J_r}\left(\tau_r - R_r F_{xr} - sign\left(\omega_r\right)\tau_{Br} - k_r v_{xr}\right) \quad , \tag{3.11}$$

where J_i is moment of inertia of the i-th wheel around its y axis; τ_i is drive torque applied by a powertrain on the i-th wheel; R_i is radius of the i-th wheel; F_{xi} is the force acting on the center of the i-th wheel along its x-axis; ω_i is angular velocity of the i-th wheel; τ_{Bi} is braking torque applied by brakes on the i-th wheel; k_i is a coefficient of the road drag for the i-th wheel; v_{xi} is the velocity vector projection of the i-th wheel's center on its x-axis.

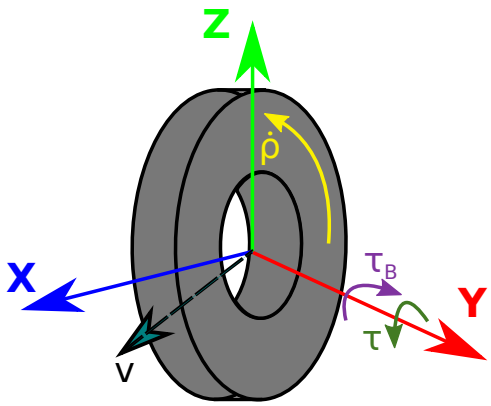

Figure 3.3: Wheel coordinate system.

3.2.2 Pacejka magic formula

Pacejka's formula introduced in [Pac02] is used for computation of the forces acting on a wheel. It is used for tire modeling. This formula contains more than 20 coefficients. This is the reason why it is not so convenient to use. It was simplified in [Haf08]. This formula requires the longitudinal slip ratio λ or tire's slip angle α from which the force F_x or F_y is determined.

Longitudinal slip ratio λ

Longitudinal slip ratio is evaluated based on ω_i and wheel travel velocity v_{xi}.

The i-th wheel travel velocity v_{xi} is computed using vehicle's side-slip angle β, the vehicle's center of mass velocity v, yaw rate of the vehicle $\dot{\psi}$ and steering angle δ_i. It is computed using following formula

$$v_{xf} = v\ cos\beta\ cos\delta_f - sin\left(\delta_f\right)\left(v\ sin\beta + l_f\ \dot{\psi}\right) \tag{3.12}$$

$$v_{xr} = v\ cos\beta\ cos\delta_r - sin\left(\delta_r\right)\left(v\ sin\beta + l_r\ \dot{\psi}\right)\ . \tag{3.13}$$

Then the longitudinal slip ratio for i-th wheel is

$$\lambda_i = \frac{v_{ci} - v_{xi}}{max\left(|v_{ci}|, |v_{xi}|\right)}\ , \tag{3.14}$$

where v_{ci} is circumferential velocity of i-th wheel which is computed as

$$v_{ci} = R_i\omega_i\ , \tag{3.15}$$

where R_i is radius of i-th wheel.

Tire's slip angle α

Slip angles α_i (where i stands for i-th wheel) are calculated using vehicle's slip-angle β, steering angles δ_i, inertial velocity v and yaw rate $\dot{\psi}$. It is

computed using the following equations (adopted from [Efr18])

$$\alpha_f = \delta_f - arctan\left(\frac{v\sin\beta + l_f\dot{\psi}}{v\cos\beta}\right) \tag{3.16}$$

$$\alpha_r = \delta_r - arctan\left(\frac{v\sin\beta - l_r\dot{\psi}}{v\cos\beta}\right) \tag{3.17}$$

Pacejka magic formula

The tires are modeled using Pacejka magic formula. The formula is

$$F_{xi}(\lambda_i) = D\ F_{zi} sin\left(C\ arctan\left(B\ \lambda_i - E\left(B\ \lambda_i - arctan\left(B\lambda_i\right)\right)\right)\right)\ , \tag{3.18}$$

where D, C, B and E are shaping coefficients, F_{zi} is normal load for i-th wheel and λ_i is slip ratio for i-th wheel. Pacejka configuration used for front wheel in longitudinal direction can be seen in the figure Fig. 3.4.

The formula (3.18) is also applicable for lateral force F_y calculation. The F_{yi} is substituted for F_{xi} and α_i for λ_i.

Coefficients used in this work are provided in Table B.1. Conservative set is used mainly. Only for riding tests the aggressive set is used. Coefficients with x index are used for F_x computation. The ones without index are used for F_y computation.

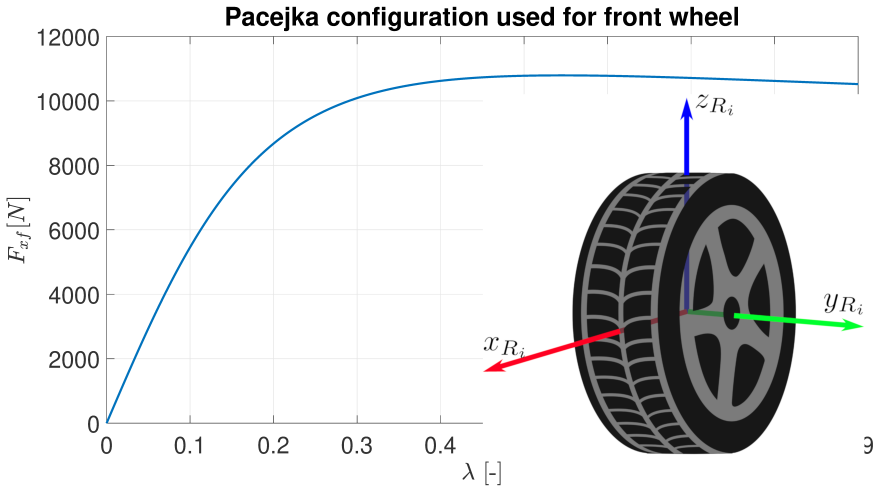

Figure 3.4: Front wheel longitudinal Pacejka model.

3.2.3 Friction ellipse

The friction ellipse is defined e.g. in [Ada]. The longitudinal and lateral forces generated by Pacejka Magic formula will be denoted as $F_{x,max}$ and $F_{y,max}$. Then the following equations (adopted from [EHH19]) are used to scale the resulting forces. Qualitative figure of friction ellipse is in Fig. 3.5.

$$\beta = \arccos\left(\frac{|\lambda|}{\sqrt{\lambda^2 + \sin^2(\alpha)}}\right), \tag{3.19}$$

$$\mu_{x,act} = \frac{F_{x,max}}{F_z}, \qquad \mu_{y,act} = \frac{F_{y,max}}{F_z}, \tag{3.20}$$

$$\mu_{x,max} = D_x, \qquad \mu_{y,max} = D_y, \tag{3.21}$$

$$\mu_x = \frac{1}{\sqrt{\left(\frac{1}{\mu_{x,act}}\right)^2 + \left(\frac{\tan(\beta)}{\mu_{y,max}}\right)^2}}, \qquad F_x = |\frac{\mu_x}{\mu_{x,act}}|F_{x,max}, \tag{3.22}$$

$$\mu_y = \frac{\tan(\beta)}{\sqrt{\left(\frac{1}{\mu_{x,max}}\right)^2 + \left(\frac{\tan(\beta)}{\mu_{y,act}}\right)^2}}, \qquad F_y = |\frac{\mu_y}{\mu_{y,act}}|F_{y,max}. \tag{3.23}$$

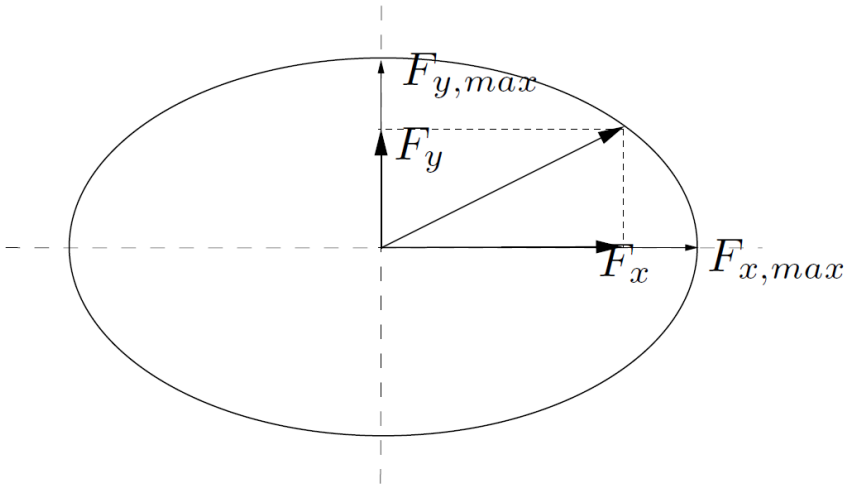

Figure 3.5: Friction ellipse example. Picture was adopted from [SHR06]

3.2.4 Powetrain

The powertrain is neglected in this model and the torque commanded with the τ_f and τ_r is considered perfectly tracked here. The motor electrical time constant is neglected and its mechanical inertia is considered to be included in wheel inertia.

3.2.5 Adopted model summary

The single-track mathematical model presented to this moment was adopted. Modifications needed for higher model fidelity are proposed in the following sections. These modifications are then used in control design process for better performance of proposed controllers.

The adopted model has overall 5 states and 6 inputs. States are:

- Velocity $|v|$.
- Side-slip angle β.
- Yaw rate $\dot{\psi}$.
- Angular velocities of both wheels - ω_f and ω_r.

Inputs to the system are:

- Engine torques τ_i.
- Breaking torques τ_{Bi}.
- Wheel steering angles δ_i.

The i stands for f - front or r - rear.

Nonlinear model that is used in LPV controller design (details can be found in Chapter 4) is the model described so far. Following sections in this chapter describe modifications that were made for angular velocity ω tracking based control system described in Chapter 5.

3.2.6 Modifications of the single-track model

The following physical phenomena are missing in the model adopted from [Efr18] and [VHH19].

- Aerodynamic drag force
- Limitations of torque and power generated by the powertrain.
- Normal force F_z disturbances.

In order to improve the model fidelity, these were added.

3.2.7 Aerodynamic drag

Drag force F_D is computed as

$$F_D = \frac{1}{2}\rho_{air}\ A\ c_D\ v^2 \quad , \tag{3.24}$$

where A is the reference frontal area, c_D is drag coefficient, v is vehicle velocity and ρ_{air} is air density. F_D is acting in opposite direction to the vehicle velocity v in the CG. Instead of v the air velocity of the vehicle should be used. This is however neglected and only vehicle velocity is considered.

3.2.8 Powertrain limits

The motor limitations on torque and power were added to the model, in order to represent more accurately the physical reality and possibilities of current state of powertrain. The limitation on torque is its maximum value. The power max value is limited based on wheel angular speed and torque. The power is computed as

$$P = \omega_i \cdot \tau_i \quad , \tag{3.25}$$

where ω_i and τ_i are i-th wheel angular velocity and torque. This impose limitation on applicable torque. Available torque as function of vehicle velocity can be seen in figure Fig. 3.6.

The dynamics of the powertrain is considered. It is modeled as a first order system with time constant $\tau = 1$ ms. This corresponds to the electrical part of the engine. The mechanical inertia of the engine is considered to be included in the wheel inertia which can be done without loss of generality.

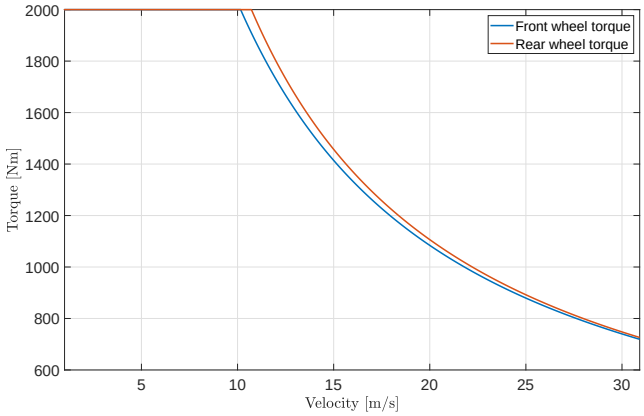

Figure 3.6: Limitations on torque applicable to the wheels. These limitations are imposed by finite torque and power of the powertrain. This figure shows the maximum applicable torques on the front and rear wheel as function of vehicle velocity. The data come from simulation of max applicable torque during acceleration. Normal force F_{zf} is smaller than F_{zr}. Regarding this fact the front wheel gets sooner to its power limits, so the ω_f is bigger than ω_r in that time. This fact and equation (3.25) are explaining behavior that can be seen in this figure. Power limits on front wheel are reached earlier. This simulation was made on surface that has quite big friction coefficient and the wheel longitudinal slip ratios λ were all the time in the linear region, that is around zero slip ratio.

3.2.9 F_z disturbances

The possibility to change the F_z force on front wheel and on the rear wheel was added to the model. With this approach some important physical phenomena (discussed later in Section 3.2.10) can be represented. Disturbance of F_{z0i} (nominal normal force on front and rear wheel respectively), where i stands for f - front or r - rear, is modeled through the introduced input $F_{zi}ratio$. The F_{zi} is then computed as

$$F_{zi} = F_{zi}ratio \cdot F_{z0i} \quad , \tag{3.26}$$

where

$$0 \leq F_{zi}ratio \leq 1. \tag{3.27}$$

3.2.10 Physical phenomena represented by the F_z disturbance

According to the Pacejka magic formula used with the friction ellipse (can be found in [EHH19]) the force generated by the wheel F_x is part of the

$F_{combined}$ force in the x direction. F_x is computed

$$F_x = \mu_x F_z \quad , \tag{3.28}$$

where μ_x is friction coefficient in x direction (equations and definitions can be found in Section 3.2.3).

Changes in μ_x can be caused by:

- Tire properties and its changes (Tire aging, different tires,...)
- Different road surfaces that the vehicle rides on.
- From the formula (3.20) is clear that it is dependent on:
  - wheel slip ratio λ
  - wheel slip angle α

For sake of simplicity variation of μ_x is modeled through variation of F_z in this work. Thus the shape of slip curve is considered constant and is scaled by F_z. Here the disturbance of F_z represents:

- Effect of friction coefficient change in lateral direction caused by side slip angle α variation. Which Can be induced by:
  - Wheel steering angle δ.
  - Vehicle side slip angle β.
- Tire properties.
- Riding surface properties.
- Disturbances in normal force F_z (like smaller F_z on front wheel during acceleration, bouncing wheel,...).

Chapter 4

Longitudinal Slip Ratio Control Using Gain Scheduling and LQ Based Methods

4.1 Introduction

As can be seen in the Chapter 3 the vehicle model is nonlinear, which means it is needed to be linearized in order to use LQ techniques. The λ_{Ref} reference signal (more on choose of the reference signal was in Chapter 2) is assumed to be piecewise constant and nonzero. It implies that also acceleration should be piecewise constant and nonzero, depending on the disturbance character (e.g. constant normal force F_z and parameters of Pacejka's magic formula ensure constant acceleration if no other disturbance is present). The velocity is state of the system. This leads to linearization outside of equilibrium (nonzero derivative of state). The acceleration has to be controlled over whole velocity range in which the operation is required. The system was linearized in velocity range 3 - 40 m/s (10 - 130 km/h).

The nonlinear model without modifications presented in Section 3.2.5 is used in this chapter.

4.2 Linearization

Brief discussion regarding linearization will be held in this section.

The desired operating region of the closed-loop system on the Pacejka slip curve (can be seen on the figure Fig. 4.1) is in the almost linear region.

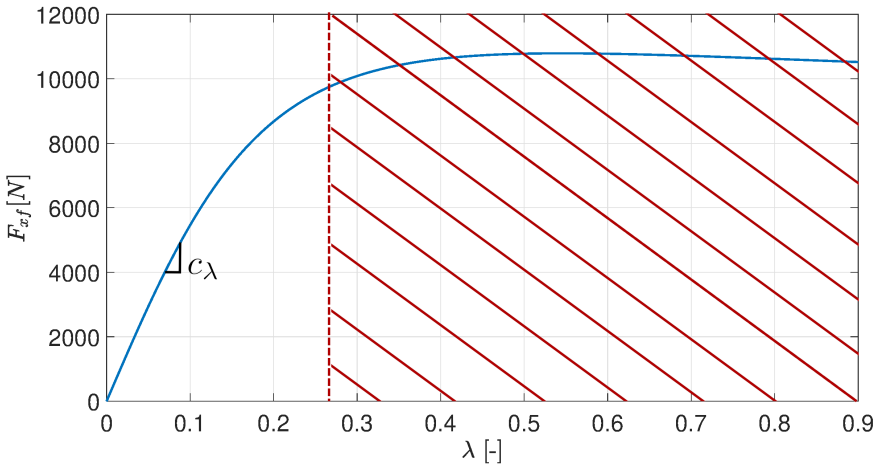

Figure 4.1: Desired, almost linear, operating region of Pacejka slip curve.

Trajectory along which the model was linearized is constant acceleration and constant wheel angular acceleration for both wheels. The linearization along trajectory creates set of linear models, which are switched based on the velocity of vehicle. This scheme leads to LPV (linear parameter varying) model usage. The switching of the models will be discussed later on. In the following subsection LPV model and algorithm used for linearization of the nonlinear model will be described.

4.2.1 LPV model

A linear parameter-varying (LPV) system is a linear state-space model with dynamics changing as function of parameters p, called scheduling parameters. It has mathematical equations

$$\frac{dx}{dt}(t) = A(p)\,x(t) + B(p)\,u(t) \tag{4.1}$$

$$y(t) = C(p)\,x(t) + D(p)\,u(t) \tag{4.2}$$

where A, B, C and D are LPV state space matrices. In scope of this work the scheduling parameter is only vehicle velocity v.

4.2.2 Linearization algorithm

Linearization algorithm used to derive linearized model will be described in this section.

The input parameters of this algorithm are velocity range, slip ratio used and linearization error tolerance. The linearization error tolerance is euclidean norm of error between nonlinear and linearized model's derivatives. The actual linearization error ERR is computed as

$$ERR = ||\dot{x}_{non-lin} - \dot{x}_{lin}||_2 \ . \tag{4.3}$$

Output of the algorithm is grid of state space models that are being switched depending on the velocity. The switching itself is described in Section 4.2.4. If linearization error tolerance parameter is smaller than ERR new linearization operating point is created. Acceleration is computed from the longitudinal force applied to the vehicle and it's mass. The longitudinal force is derived from wheel slip ratio using the Pacejka magic formula.

The linearization algorithm takes initially the lowest velocity from the velocity range that has to be linearized. From the velocity and slip ratio, which is specified as parameter, the wheel angular velocity and angular acceleration is computed. With these information the operating point search can be launched.

Operating point search

The operating point (OP) is found using numerical methods. The cost function $L\left(x, \dot{x}, u, \dot{x}_{desired}\right)$ is introduced where the nonlinear equations from the model are used to compute the derivatives depending upon the state and inputs. $L\left(x, \dot{x}, u, \dot{x}_{desired}\right)$ equals to weighted square of difference between the desired derivatives and computed ones:

$$\dot{x}_{diff} = \dot{x}_{desired} - \dot{x}_{nonlin}\left(x_{OP}, \dot{x}_{OP}, u_{OP}\right) \tag{4.4}$$

$$L\left(x, \dot{x}, u, \dot{x}_{desired}\right) = \dot{x}_{diff}^{T} \cdot weight \cdot \dot{x}_{diff} \quad , \tag{4.5}$$

where $x_{OP}, \dot{x}_{OP}$ and u_{OP} are operating point values, $weight$ is matrix of weights (identity matrix was used in this thesis) and $\dot{x}_{desired}$ are derivatives of the trajectory along which the system is linearized. Fixed states and input

values are soft fixed (there is ±1% tolerance in the fixed values) in order to find feasible operating point. These fixed states are velocity and wheel angular velocity of both wheels. Then the algorithm performs minimization (using MATLAB's function *fmincon*) of the cost function.

Linearization

At this moment the OP has been already found. The actual linearization is done using MATLAB's *linmod* command and simulink implementation of nonlinear model which was described in the section Section 3.2.5.

This way the state space representation is derived. The algorithm adds to the current working velocity increment, as described in Section 4.2.2, and checks if the ERR value is sufficiently small (see equation (4.3)). If so, the increment is iteratively added and the ERR value is checked until either the ERR value is higher than the specified tolerance or velocity v exceeds the velocity range specified as input to the algorithm. In the latter case the algorithm is terminated. In the first case, the algorithm repeats the trimming step (noted in Section 4.2.2). The linearization algorithm flowchart is shown in figure Fig. 4.2.

4.2.3 Linearized model

The linearization was created in a grid parameterized by longitudinal velocity in range from 3 m/s to 40 m/s. Using longitudinal slip ratio 0.15 and error tolerance equal to 3 i.e. it should always be true that $ERR \leq 3$ (see the above sections for detailed informations on the algorithm and its variables).

Using these parameters array of 53 state space models was derived. These state space models describe only behavior of incremental model

$$\frac{d\Delta x}{dt} = A\left(p\right)\Delta x + B\left(p\right)\Delta u \tag{4.6}$$

$$\Delta y = C\left(p\right)\Delta x + D\left(p\right)\Delta u\ . \tag{4.7}$$

The algorithm's output are also offsets of states derivatives dx_0, inputs u_0 and states x_0. The input to the system u is then $u = u_0 + \Delta u$.

As the system was linearized along trajectory the output of the incremental model must be added to the trajectory. The trajectory is being reconstructed using the $dx_0(p)$ values obtained from the linearization algorithm. These values being integrated will provide the trajectory which is then added to the system output. This practice can be done as the derivatives are known along the whole trajectory - trajectory can be reconstructed, if it wouldn't be the case whole trajectory would have to be also output of the algorithm.

The whole model can be described by incremental model (equations (4.6) and (4.7)) and by equations

$$u = u_0(p) + \Delta u \tag{4.8}$$
$$y = \Delta y + trajectory \tag{4.9}$$

4.2.4 Switching of the models

Switching of the models is quite straightforward. Out of the exact points on grid of trimmed velocities the weighted average of two nearest models is used (convex combination). The weight is computed as

$$w = \frac{v - grid(i)}{grid(j) - grid(i)} \tag{4.10}$$

where $j = i + 1$, i is index in the grid of velocities of the closest smaller velocity to the current vehicle velocity v (briefly $v > grid(i)$). Then the values for the variables dependent on the switching variable v are computed as

$$a_{kl}(p) = (1 - w) \cdot a_{kl}(i) + w \cdot a_{kl}(j) \ , \tag{4.11}$$

where w is the weight from (4.10), a stands for generic switched variable that is sampled in a grid of velocities and $A(p)$ stands for that variable used in the LPV model (eg. state space matrix $B(p)$).

Due to inaccurate trim of the nonlinear model, the switching wouldn't be bump-less if the system would be switched as it was described above. So the generated system matrices' and operating points' values were fitted with polynomial curve. The eight order polynomial was used. The robust bisquare method was used for fitting. Example of fitted yaw rate operating point, which is state of system, can be seen in the figure Fig. 4.3. Using the fitted curves' values in the velocity grid points new system matrices and operating points' values were generated. These values are then used in switching as was described in equation (4.11).

4.3 LQ based control

For the grid of state space models also a grid of gains was computed. The weights were tuned experimentally. This grid of gains is switched similarly as in the case of state space switching described in section Section 4.2.4.

The control architecture is depicted on the figure Fig. 4.4. Because of the requirment of zero error signal $e = \lambda_i - r$, where λ_i is i-th slip ratio, the extra integrals have been added to the system. Then the Q matrix is set up so, that the state of the integrated error goes to zero. This is achieved simply by extending the system in following way

$$\begin{bmatrix} \dot{x} \\ \dot{x}_i \end{bmatrix} = \begin{bmatrix} A & 0 \\ C & 0 \end{bmatrix} \begin{bmatrix} x \\ x_i \end{bmatrix} + \begin{bmatrix} B \\ 0 \end{bmatrix} \begin{bmatrix} u \\ 0 \end{bmatrix} + \begin{bmatrix} 0 \\ r \end{bmatrix} \tag{4.12}$$

$$\dot{x}_{aug1} = A_{aug1} \cdot x_{aug1} + B_{aug1} \cdot u_{aug1} \ , \tag{4.13}$$

where r is reference and from the control design point of view it is taken as disturbance and is not considered in the design of LQ controller. The x is state of the LPV system and x_i is state of the added integral. Input of this integral is the error signal e. Second thing, that is done in the architecture and can also be seen on the block diagram are input filters.

Input filters were added in order to control the frequency response of the input to the system. This was done so as continuous control actions were reached. These are considered to be first order filters. The extension of the system is again straightforward

$$\begin{bmatrix} \dot{x}_{aug1} \\ \dot{x}_{filter} \end{bmatrix} = \begin{bmatrix} A_{aug1} & B_{aug1} \\ 0 & -B_{filter} \end{bmatrix} \begin{bmatrix} x_{aug1} \\ x_{filter} \end{bmatrix} + B_{filter} \cdot u_{filter} \ , \tag{4.14}$$

where x_{filter} is state of the filters and B_{filter} is diagonal matrix with one over time constants $1/\tau$ of the applied filters. In this work $\tau = 10^{-3}s$ is used.

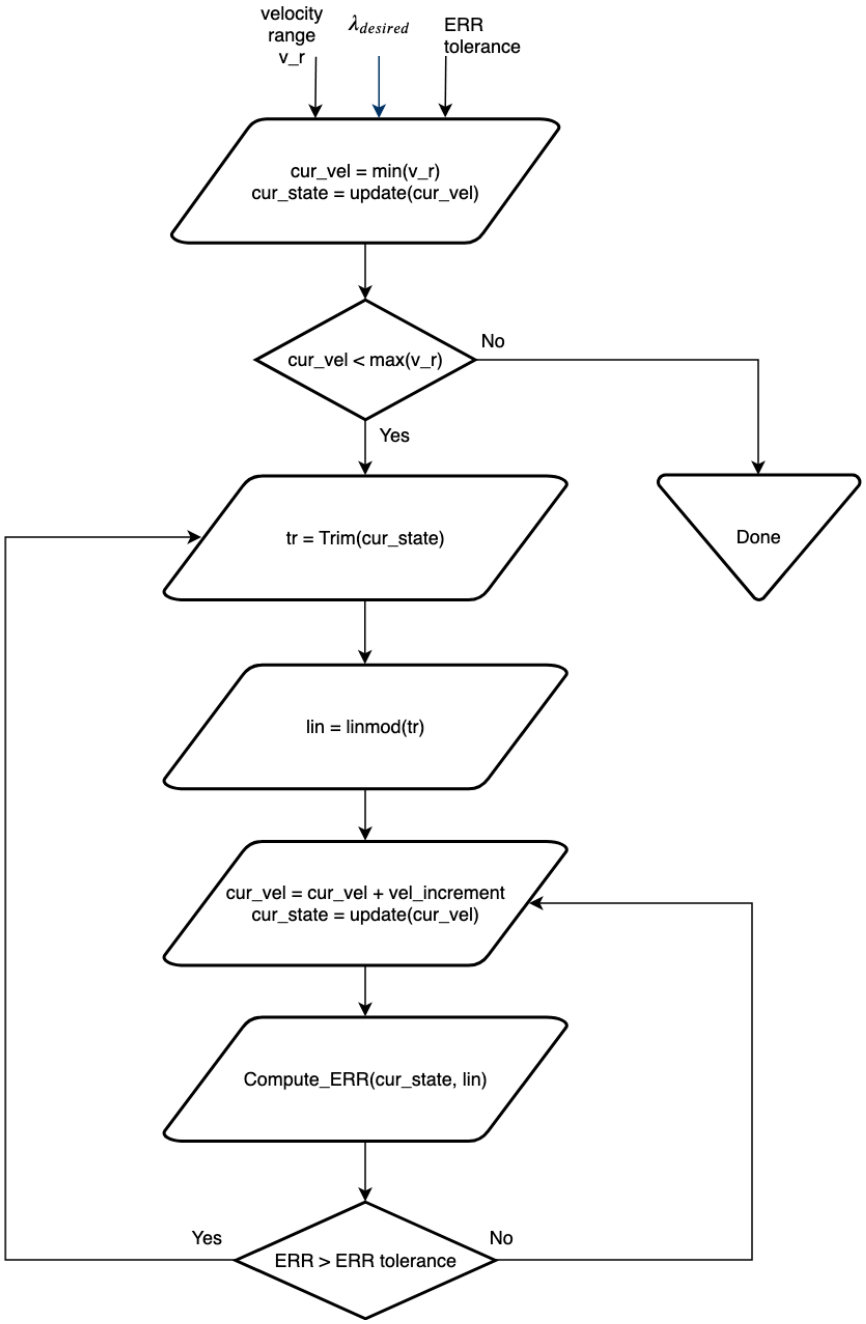

Figure 4.2: Flowchart of the linearization algorithm developed.

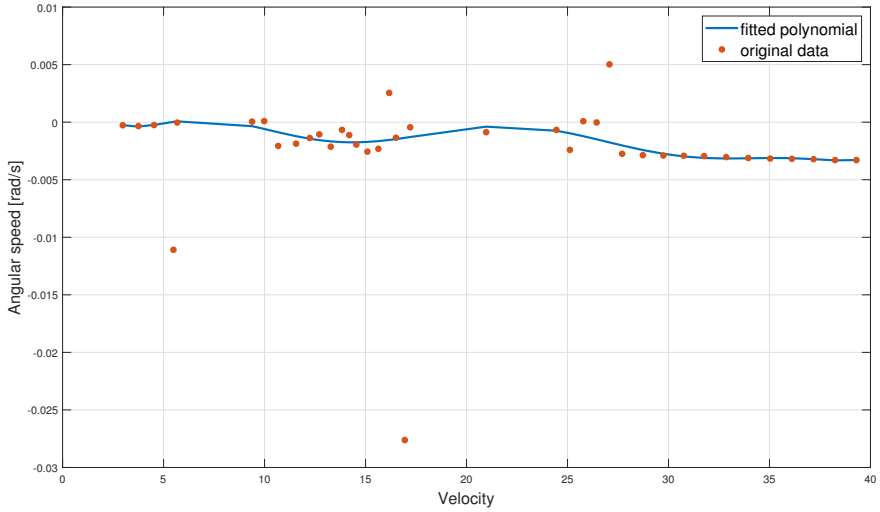

Figure 4.3: Yaw rate fitted polynomial as function of vehicle velocity.

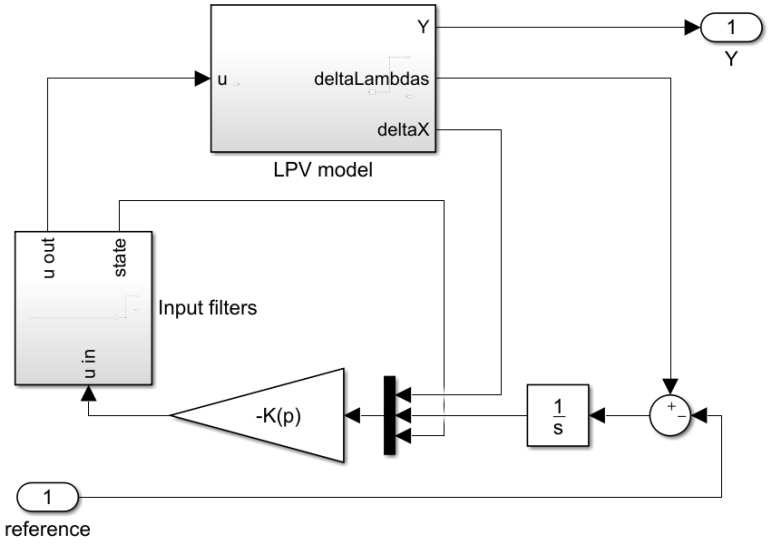

Figure 4.4: Block diagram of the control architecture based on LPV model.

Chapter 5

Acceleration/Longitudinal Slip Ratio Control Using Wheel Angular Velocity Tracking with LQ Techniques

In this chapter alternative architecture of slip ratio λ/vehicle acceleration control is presented. Here presented approach is more complex (more on this in Section 5.1.4) and it brings quite satisfactory results that are verified in Chapter 6.

5.1 Control architecture

The hierarchical control system has following structure. The ω controller is core controller. Reference for it is computed in "ω reference generator" and it is computed based on λ demand that comes from the most top structure - the acceleration controller.

Longitudinal slip ratio λ is according to the Pacejka magic formula (see [Pac02] or [VHH19]) "generating" the traction force. If we restrict ourselves on the linear region then the λ is directly proportional to the acceleration. Fortunately the value of maximum allowable λ is not much wandering with the change of riding conditions like surface friction, tire aging, et cetera (see again [Pac02]).

The acceleration controller block diagram, which is P controller, is shown in the figure Fig. 5.1. This is classical methods based controller with not the performance that would have some advanced methods based controller (like LQ), but it is very simple.

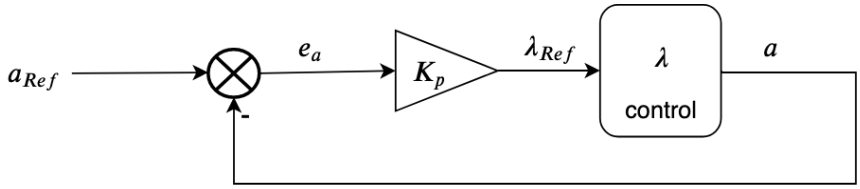

Figure 5.1: Block diagram of acceleration feedback loop with P controller used.

Single-track model has dominant nonlinearity in the slip ratio λ which has to be tracked. λ is computed using following equation

$$\lambda = \frac{\omega r - v}{max\left(|v|, |\omega r|\right)} \quad . \tag{5.1}$$

Regarding this nonlinearity the first thought was to create LPV model and controller for it (see [VHH19] and Chapter 4). This chapter presents alternative control architecture.

The block diagram of the proposed control architecture is in the figure Fig. 5.2.

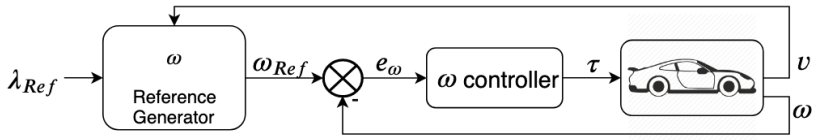

Figure 5.2: The block diagram with the λ control system architecture.

5.1.1 ω reference generator

The "ω reference generator" handles the nonlinearity in the single track model. As it comes from the name of this block, it generates the ω_{Ref} that is used as reference for the feedback controller described in Section 5.1.3. It has input λ_{Ref} and parameter v. From these is according to the λ_{Ref} sign the ω_{Ref} computed.

If $\lambda_{Ref} > 0$ then

$$\omega_{Ref} = \frac{v}{(1 - \lambda_{Ref})\ r} \quad , \tag{5.2}$$

where v is vehicle velocity and r is diameter of the wheel.

If $\lambda_{Ref} < 0$ then

$$\omega_{Ref} = \frac{(\lambda_{Ref} + 1)\ v}{r} \quad . \tag{5.3}$$

This ω reference generator is used twice. First for the front wheel and second for the rear wheel.

5.1.2 Design model

Design model is the nonlinear model that is linearized in operating point, and used for the feedback control design. Only two states ω_f and ω_r are considered in the design model. The vehicle model dynamics is then transformed to the following equation

$$\dot{\omega}_i = \frac{1}{I + ratio_i\ m\ \ (1 \pm \lambda_i)\, r_i^2} \cdot (\tau_i - ratio_i\ F_d\ r) \quad , \tag{5.4}$$

where I is inertia of the wheel, $ratio_i$ is ratio of the mass which is driven by the i-th wheel, m is whole mass of the vehicle, $lambda_i$ is i-th slip ratio demand, r_i is diameter of the i-th wheel, τ_i is i-th moment applied to the i-th wheel (this is input to the system and comes from the engine) and F_d is aerodynamic drag.

The part of this equation where the inertia of wheel is extended by the mass of the vehicle comes from well know equations

$$F = m\ a \quad , \tag{5.5}$$

$$M = F\ r \quad , \tag{5.6}$$

$$v = (1 \pm \lambda)\, \omega\ r \implies a = (1 \pm \lambda)\, \dot{\omega}\ r \tag{5.7}$$

$$F = m\ \ (1 \pm \lambda)\, \dot{\omega}\ r \tag{5.8}$$

$$M = m\ \ (1 \pm \lambda)\, \dot{\omega}\ r^2 \tag{5.9}$$

$$M = I\ \dot{\omega} \implies I = m\ \ (1 \pm \lambda)\ \ r^2 \quad . \tag{5.10}$$

The equation (5.7) is valid under assumption that λ is constant. The equation for F_d was already mentioned in equation (3.24), where the velocity is replaced using equation (5.7). So the whole equation is

$$ratio_i\ F_d = ratio_i\ \frac{1}{2}\rho_{air}\ A\ c_D\ \left((1 \pm \lambda_i)\ \omega_i\ r_i\right)^2 \quad . \tag{5.11}$$

All other physical phenomena are assessed as disturbances. These are mainly:

- Pacejka magic fromula coefficients - different types of tires, riding surfaces,...
- Disturbances coming from the nature of the operation:
  - Normal force disturbances - wheel goes through hole
  - Disturbances in control action (torque) - vehicle goes to the hill
- Lateral dynamics effect on longitudinal motion (mainly the effect of the friction ellipse as described in [EHH19] and in Section 3.2.3).

5.1.3 ω controller

Reference coming to ω controller will be from it's nature (see Section 5.1.1) hyperbolic. Provided this fact the controller contains two integrators in order to be able of the reference tracking with zero steady state error. The controller is designed to use only the τ_f and τ_r. This is because only the acceleration is in the scope of this work.

Controller was developed using LQ techniques. The LQ gain was computed for augmented system as two integrators were added. It's state space matrices A_{aug} and B_{aug} are

$$A_{aug} = \begin{pmatrix} A & 0 & 0 \\ C & 0 & 0 \\ 0 & I & 0 \end{pmatrix}, B_{aug} = \begin{pmatrix} B \\ D \\ 0 \end{pmatrix} \quad , \tag{5.12}$$

where the A, B and C are state space matrices of the linerized design model (described in Section 5.1.2).

ω_i which are regulated (brought to zero) are in fact differences of the ω_i and it's reference in the control system architecture.

5.1.4 Controller summary

Alternative (let us say "robust") approach compared to the controller proposed in the Chapter 4 is presented in this chapter. The "robust" means the ω tracking controller is able to follow ω_{Ref} coming form the ω reference generator. The behavior was explored experimentally in simulation environment (see the Chapter 6). Both of these controllers are solving the same problem. The biggest advantage of this controller is its invariance to vehicle velocity v. It is also much simpler which brings many advantages like better implementation, tuning, error proneness and so on.

Chapter 6

Results

Longitudinal slip ratio/acceleration controllers were introduced in previous chapters. In this chapter their verification and comparison of them will be shown. Also virtual riding tests made using vehicle dynamics blockset toolbox in Simulink will be shown here.

6.1 Gain scheduling controller

In this subsection results using the controller from Chapter 4 are presented.

The designed controller was tested with two different scenarios. The testing of the controller was done using the adopted non-linear model (see Section 3.2.5). The first test case was to slightly modify the Pacejka model in order to test controller robustness. The time response of the controller can be seen on the figure Fig. 6.3 for the front wheel and on the figure Fig. 6.4 for the rear wheel. On these figures are also for better insight the Pacejka models of the non-linear model against which the controller was tested. Here, on the Pacejka curves, are also depicted the operating regions of the system. Three cases were considered. Pacejka model for which the system was designed, then the same one but with the D coefficient 1.3 times bigger and the last one was also the same as the for which the system was linearized but with 70% of the original D coefficient. The second test case was inputs' disturbance rejection. The rejection of disturbance can be seen on the figure Fig. 6.1 for the front wheel and on the figure Fig. 6.2 for the rear

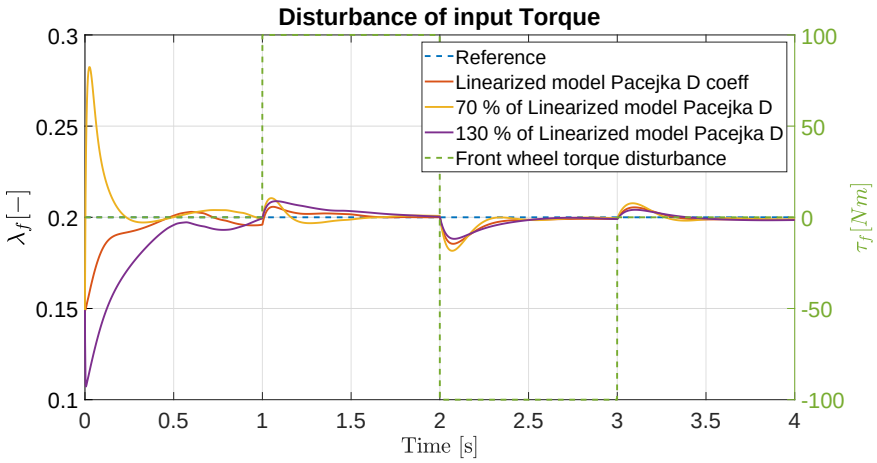

Figure 6.1: Response of the designed controller to disturbance. On this figure is slip ratio of front wheel.

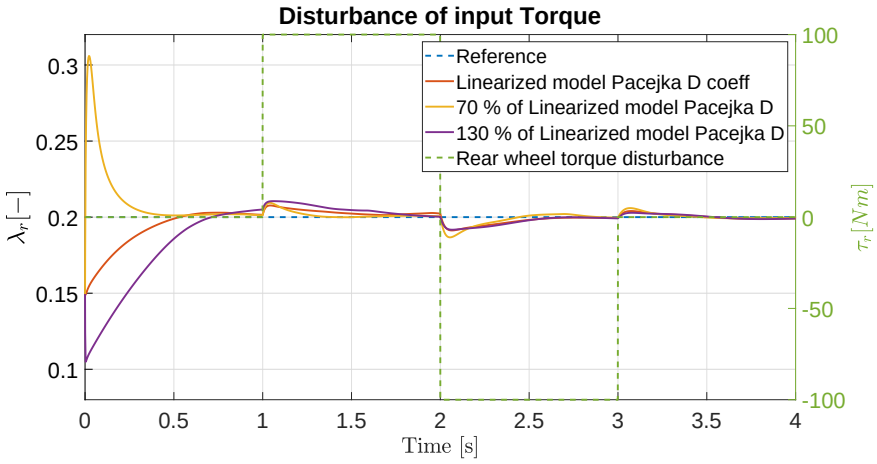

Figure 6.2: Response of the designed controller to disturbance. On this figure is slip ratio of rear wheel.

wheel. The disturbance is realized as addition of disturbance signal to the applied torque from controller. The same three Pacejka model configuration which were used in the first test scenario were used.

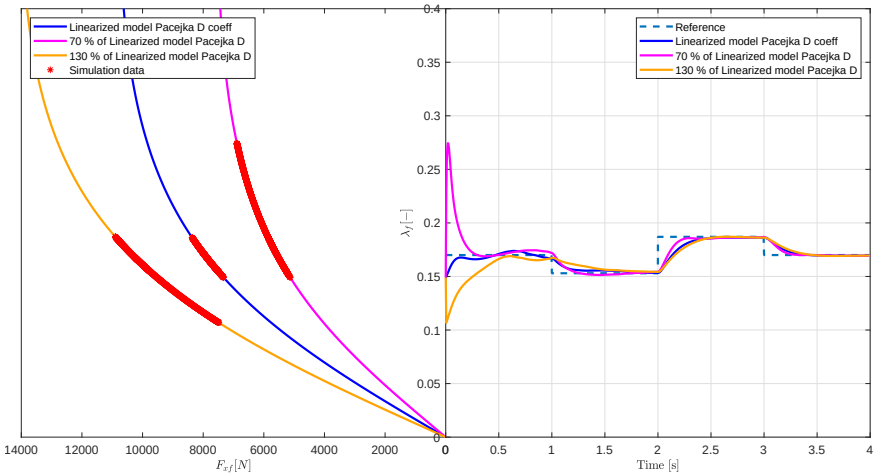

Figure 6.3: Comparison of the designed regulator for different Pacejka model of tires/road. On this figure is slip ratio of front wheel. On the left part of the figure are different Pacejka models. The simulation data points shows the operating range of the slip ratio respectively longitudinal force. On the right part of the figure the corresponding time response is shown.

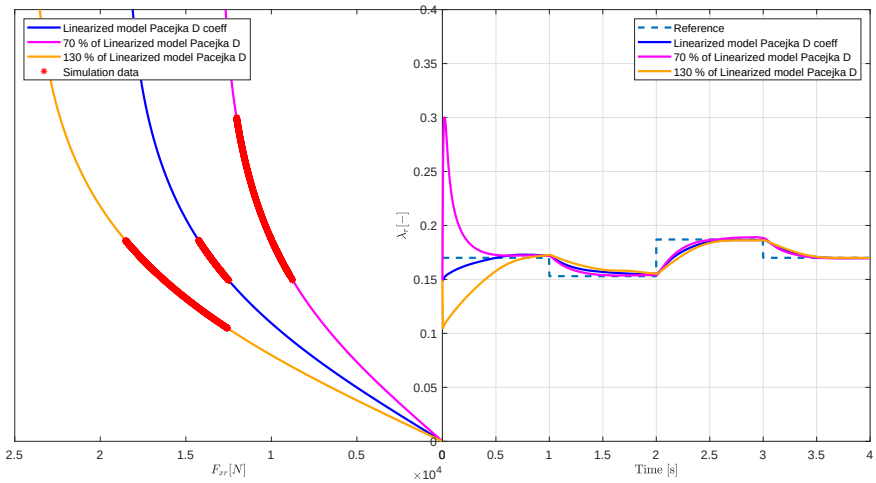

Figure 6.4: Comparison of the designed regulator for different Pacejka model of tires/road. On this figure is slip ratio of rear wheel. On the left part of the figure are different Pacejka models. The simulation data points shows the operating range of the slip ratio respectively longitudinal force. On the right part of the figure the corresponding time response is shown.

6.2 ω tracking based control system

Results made with the control system proposed in chapter Chapter 5 are presented in this section.

The proposed control system architecture was verified using the modified single-track model described in Chapter 3. The front wheel control system performance and robustness properties can be seen in the figure Fig. 6.7a. The same situation but for the rear wheel can be seen in the figure Fig. 6.7b. λ tracking details for front and rear wheel respectively can be seen in the figures Fig. 6.5 and Fig. 6.6. These figures of details are comparable to figures Fig. 6.3 and Fig. 6.4 made using the gain scheduling based controller.

With the proposed controller the following was achieved

- The traction control that has function of nowadays widely used ASR (anti slip regulation) is designed.
- The controller is invariant to significant changes of F_z (Change from 10% to 120% of the nominal F_{z0} is shown in the figures Fig. 6.7a and Fig. 6.7b). That means the controller is invariant to:
  - change of vehicle mass
  - different F_z on front and rear wheel which means invariant to center of gravity location.
  - cornering maneuvers with acceleration and generally it is usable with nonzero value of α.

Results are more in detail inspected in the following subsections.

6.2.1 Front wheel

The most important variables regarding the front wheel during the vehicle acceleration can be seen in the figure Fig. 6.7a. If it is not said else this section will describe this figure. The vertical red dashed line, that is present in all graphs, is the moment where engine reaches its power limit and is no more capable of λ tracking.

The acceleration reference a_{Ref} and its real value a can be seen in the second graph. The velocity v is also shown in this graph. Ideally the ramp of v wouldn't be dependent on the $F_{zf}ratio$, but in the time where $F_{zf}ratio$ goes to 10% (this can be e.g. as the vehicle goes on ice) the maximal possible acceleration is not sufficient and the controller isn't capable of a_{Ref} tracking. This is caused by the saturation in the λ_{Ref}. λ_{Ref} is limited to linear region

of the Pacejka's slip curve (more about this in [VHH19]). λ_{Ref} is saturated on ± 0.17 in this thesis, where the maximal F_x is generated.

$F_{zf}ratio$ and ω tracking is shown in the first graph. There are three remarkable parts. At the beginning the reference has hyperbolic character, after that it goes to ramp. After the red dashed line the power of the powertrain is on its limits and so the controller isn't capable to track the ω_{Ref}.

λ tracking is shown in the third graph. As was written above, when the $F_{zf}ratio$ goes to 10% the λ_{Ref} is saturated on its maximal value. Comparing the figure Fig. 6.7a to the figure Fig. 6.7b the power limits are reached earlier in the latter one, approximately at 4.3s. This can be also seen in the third chart of Fig. 6.7a. The slip ratio demand λ_{Ref} ramps up because the rear wheel isn't anymore capable to generate sufficient acceleration force from that time. Till that moment the λ_{Ref} is piece-wise constant.

In the last graph torque applied to the front wheel is shown. That is the actual control action used as input to the plant - vehicle.

6.2.2 Rear wheel

The most important variables regarding the rear wheel during the vehicle acceleration can be seen in the figure Fig. 6.7b.

Most of this figure content is nearly the same as for the front wheel (described in section Section 6.2.1). Taking this fact into account only the differences will be described here.

The nominal normal force F_{z0R} that is almost twice as big as F_{z0F} makes the biggest difference. This is the reason of the red dashed line position. It is approximately at 4.3s for the rear wheel while for the front one approx. at time 5.3s.

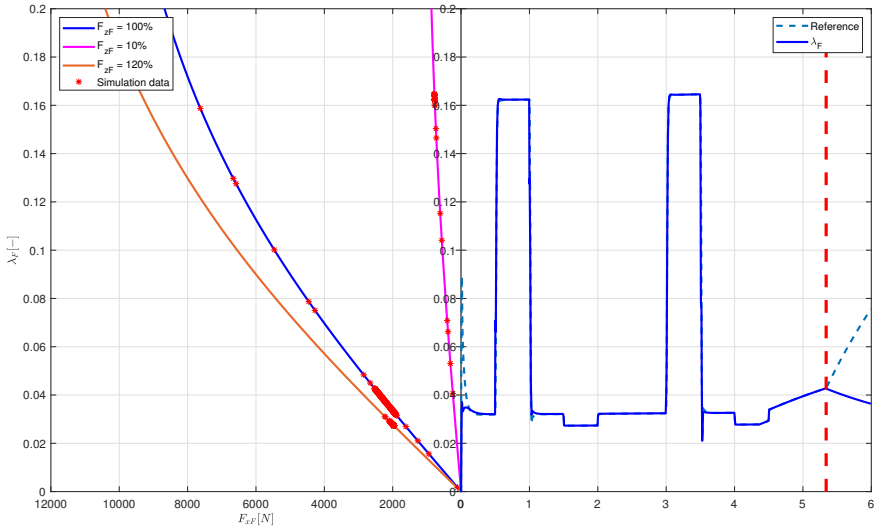

Figure 6.5: λ_f tracking results using the proposed control architecture. The inability to track the reference in higher speed (later in the time) is caused by the power limitations on the wheels.

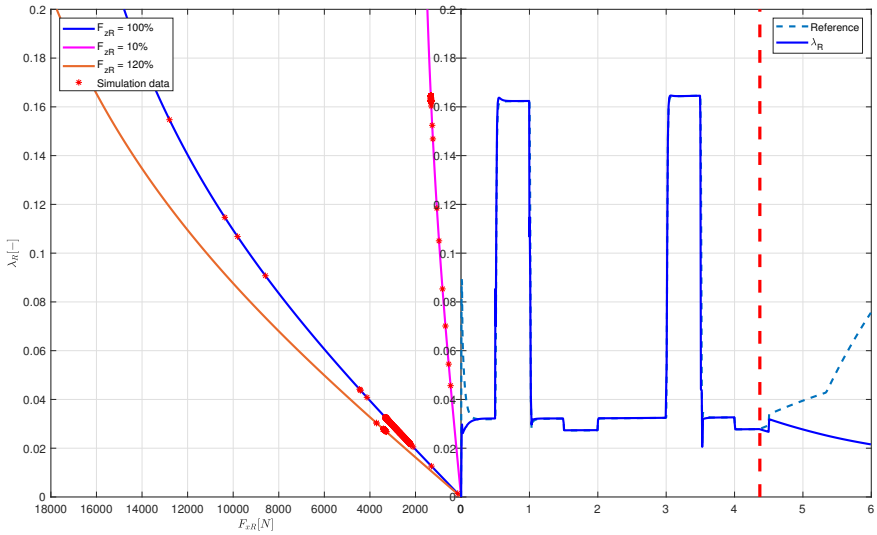

Figure 6.6: λ_r tracking results using the proposed control architecture. The inability to track the reference in higher speed (later in the time) is caused by the power limitations on the wheels.

6.3 Control systems comparison

Both proposed control systems were verified against the single-track model that was described in Chapter 3. Both of the control systems are capable of

λ tracking and disturbance rejection. Compared to each other the ω tracking based control system exhibits better performance results. It has also major advantage compared to the gain scheduling controller - It is vehicle velocity invariant.

Regarding these facts only the ω tracking based control system was chosen for virtual riding tests that are described in the following section.

6.4 Riding tests

The virtual Riding tests, which are presented in this section, are made using the Vehicle dynamics blockset (Toolbox in MATLAB/Simulink environment). As was mentioned in Section 6.3 the tests are made testing only the ω tracking based control system. There is a comparison between the variants with traction control and in open loop. The riding tests are made using university simulator that is shown in the figure Fig. 6.8.

Here is no comparison to the currently implemented ESP/ABS systems that also have sort of slip ratio control. This is because no Simulink based implementation was available.

The virtual riding test input is the driver computer interface (can be seen in the figure Fig. 6.8). The simulation of the vehicle is done using single-track model and visualization is made using the vehicle dynamics blockset.

6.4.1 Comparison of open loop and ω tracking based control system

To make also some simple nice comparable results the following scenario was set up. The driver interface was disconnected and the situation with full accelerator pedal command was simulated. That means highest a_{Ref} for ω tracking control system and full torques τ_f and τ_r for the open loop system. The inputs (τ_f and τ_r) and wheel angular speed can be seen for both variants in the figure Fig. 6.9. In the figures Fig. 6.11 and Fig. 6.12 can be seen slip ratios and Pacejka slip curve, that was slightly modified for this test (it corresponds to some slippery surface like ice). The resulting difference in vehicle velocity is depicted in the figure Fig. 6.10. Here it can be seen that

the final velocity is approximately 33 m/s for the control system against the 13 m/s for the open loop system.

A video from this virtual ride is in attachment (details in Appendix C).

6.5 Conclusion

Vehicle traction control using LQ based controllers (control architectures) was proposed with two alternative approaches in this work. As the single-track model is nonlinear global stability results should be provided if possible. In this work the global stability was tested only experimentally, no rigorous proof was presented. The approach of this work brings many benefits that were described in Section 6.2. The single-track model is in some ways simplified model (contains only 2 wheels) and for implementation in real vehicle it should be (at least according to my opinion) tested against the twin-track model (derived in [Cib19]), but overall results looks promising.

Also virtual riding tests interface was implemented. This brings opportunity to test the proposed control solutions with real driver operating the platform (see picture Fig. 6.8).

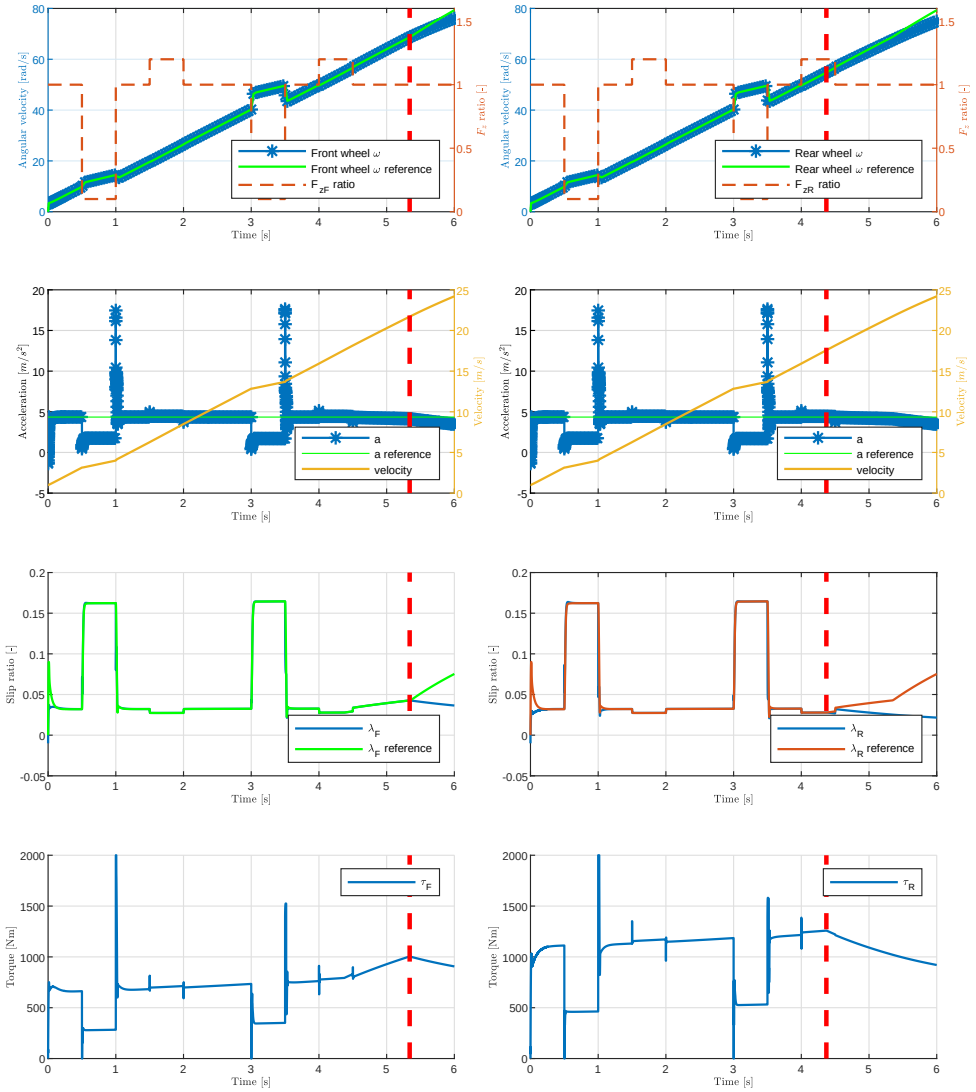

(a) : This figures presents the most important variables for the front wheel during the F_z force disturbance. Detailed description can be found in section Section 6.2.1.

(b) : This figures presents the most important variables for the rear wheel during the F_z force disturbance. Detailed description can be found in section Section 6.2.2.

Figure 6.7: Performance and robustness of proposed control architecture.

Figure 6.8: Platform used for virtual riding tests.

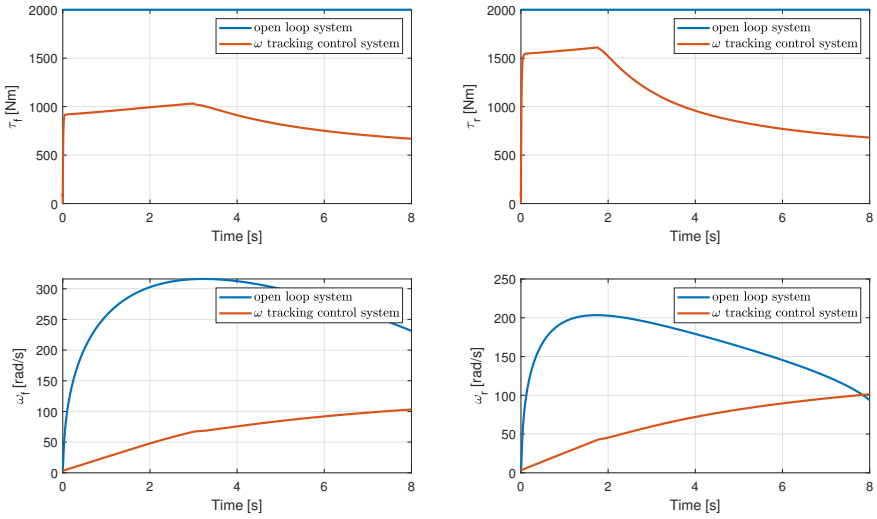

Figure 6.9: Comparison of inputs (τ_f and τ_r) and wheel angular velocities during the test with open loop system and using ω tracking based control system. Left figures are for front wheel and right for the rear one.

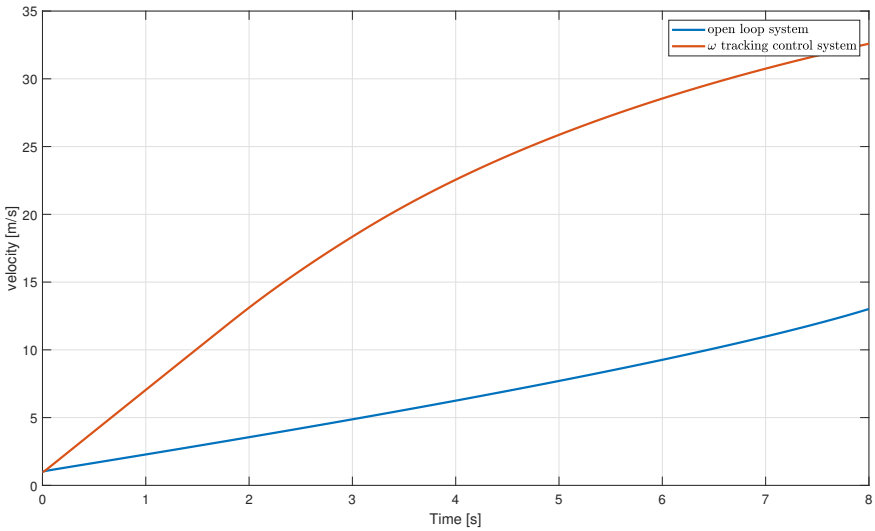

Figure 6.10: Comparison of vehicle velocity during the test with open loop system and using ω tracking based control system.

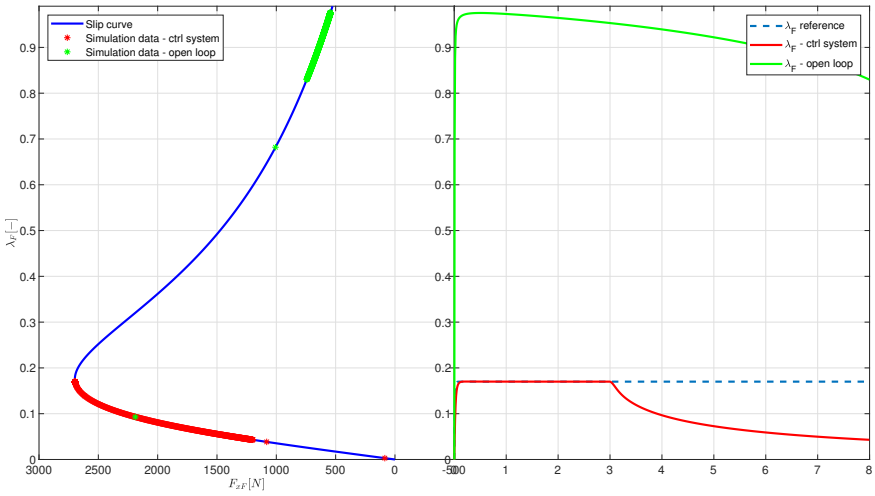

Figure 6.11: Comparison of slip ratios of front wheel during the test with open loop system and using ω tracking based control system.

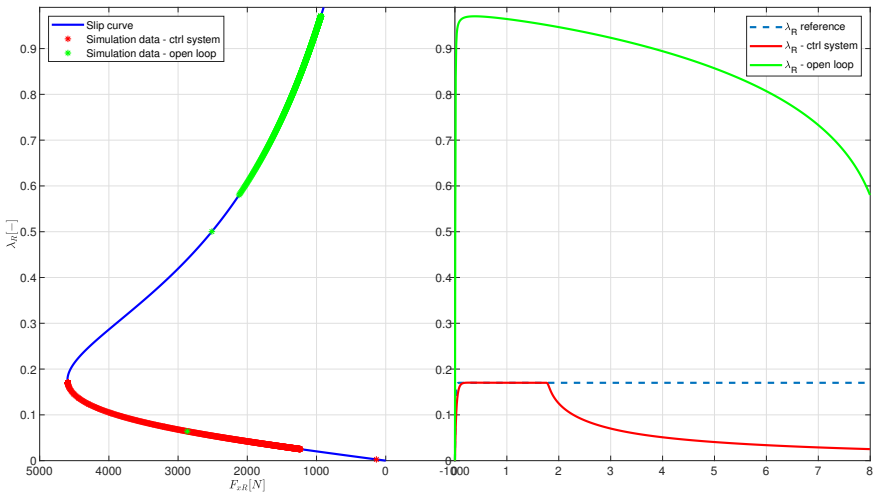

Figure 6.12: Comparison of slip ratios of rear wheel during the test with open loop system and using ω tracking based control system.

Appendix A

Bibliography

[Ack94] Jürgen Ackermann, *Robust decoupling, ideal steering dynamics and yaw stabilization of 4ws cars*, Automatica **30** (1994), no. 11, 1761–1768.

[Ada] Adams/Tire, *Using the pac2002tire model.*

[Cib19] Vit Cibulka, *Mpc based control algorithms for vehicle control*, 2019.

[Efr18] Denis Efremov, *Unstable ground vehicles and artificial stability systems*, 2018.

[EHH19] Denis Efremov, Tomas Hanis, and Martin Hromcik, *Introduction of driving envelope and full-time-full-authority control for vehicle stabilization systems*, 2019 22nd International Conference on Process Control (PC19), IEEE, jun 2019.

[GC03] Ryszard Gessing and Adam Czornik, *About relation between lq and h2 optimal control with output feedback*, vol. 4, 07 2003, pp. 3508 – 3512 vol.4.

[GGK08] Bilin Aksun Guvenc, Levent Guvenc, and Sertaç Karaman, *Robust yaw stability controller design and hardware-in-the-loop testing for a road vehicle*, IEEE Transactions on Vehicular Technology **58** (2008), no. 2, 555–571.

[Haf08] Lukas Haffner, *Real-time tire models for lateral vehicle state estimation*, na, 2008.

[Pac02] Hans Pacejka, *Tyre and vehicle dynamics*, Elsevier LTD, Oxford, 2002.

[SHB14] Dieter Schramm, Manfred Hiller, and Roberto Bardini, *Vehicle dynamics*, Springer Berlin Heidelberg, 2014.

[SHR06] Brad Schofield, Tore Hägglund, and Anders Rantzer, *Vehicle dynamics control and controller allocation for rollover prevention*, 11 2006, pp. 149 – 154.

[SS05] Ian Postlethwaite Sigurd Skogestad, *Multivariable feedback control*, John Wiley & Sons, 2005.

[VHH19] David Vosahlik, Tomas Hanis, and Martin Hromcik, *Vehicle longitudinal dynamics control based on lq*, 2019 22nd International Conference on Process Control (PC19), IEEE, jun 2019.

[WA98] Long Wang and J Ackermann, *Robustly stabilizing pid controllers for car steering systems*, Proceedings of the 1998 American Control Conference. ACC (IEEE Cat. No. 98CH36207), vol. 1, IEEE, 1998, pp. 41–42.

[ZLH+17] Ronghui Zhang, Kening Li, Zhaocheng He, Haiwei Wang, and Feng You, *Advanced emergency braking control based on a nonlinear model predictive algorithm for intelligent vehicles*, Applied Sciences **7** (2017), 504.

Appendix B

Parameters of used vehicle models

Vehicle body parameters

Name	Value	Unit	Description
m	1190	kg	mass of vehicle body
g	9.81	m/s^{-2}	gravitational constant
I_z	1141	$kg \cdot m^2$	moment of inertia in z-axis
R_r	0.33	m	rear wheel radius
R_f	0.33	m	front wheel radius
J_r	1	$kg \cdot m^2$	rear wheel inertia
J_f	1	$kg \cdot m^2$	front wheel inertia
c_D	0.33		aerodynamic drag coefficient
A	2	m^2	aerodynamic reference area
P_{max}	69	kW	maximum engine power (for each engine)
τ_{max}	2000	Nm	maximum engine torque (for each engine)
l_f	1.1092	m	front wheel distance from CG
l_f	1.8908	m	rear wheel distance from CG
F_{z0f}	4316.4	N	front wheel nominal normal force
F_{z0r}	7357.5	N	rear wheel nominal normal force
ρ_{air}	1.22	kg/m^3	air density - approx value by the sea level

Tire parameters (Pacejka coefficients). Aggressive set used in Section 6.4.1, conservative everywhere else.

	Conservative set	Aggressive set
B	0.15	0.4
C	2	2
D	1	1
E	0.95	0.1
Bx	4	3.5
Cx	1.4	3.1
Dx	2.5	2.5
Ex	0.1	0.95

Table B.1: Pacejka magic formula coefficients sets.

Appendix C

Attached files

Attached files on CD are described in the following table.

Path	Description
Virtual riding test.mp4	Video from the virtual riding test (see Section 6.4.1).
LPV	Folder with MATLAB/Simulink implementation of control system described in Chapter 4.
LPV/functions LPV/linearization and trimming	These folders contains m-functions needed for the LPV based model execution.
LPV/LPV_init.mat	Stored values that need to be loaded to the MATLAB workspace before LPV based control simulation execution.
omegaTracking	Folder with MATLAB/Simulink implementation of control system described in Chapter 5.
omegaTracking/omegaTracking.mat	Stored values that need to be loaded to the MATLAB workspace before ω tracking based control simulation execution.

Table C.1: Attached files description.